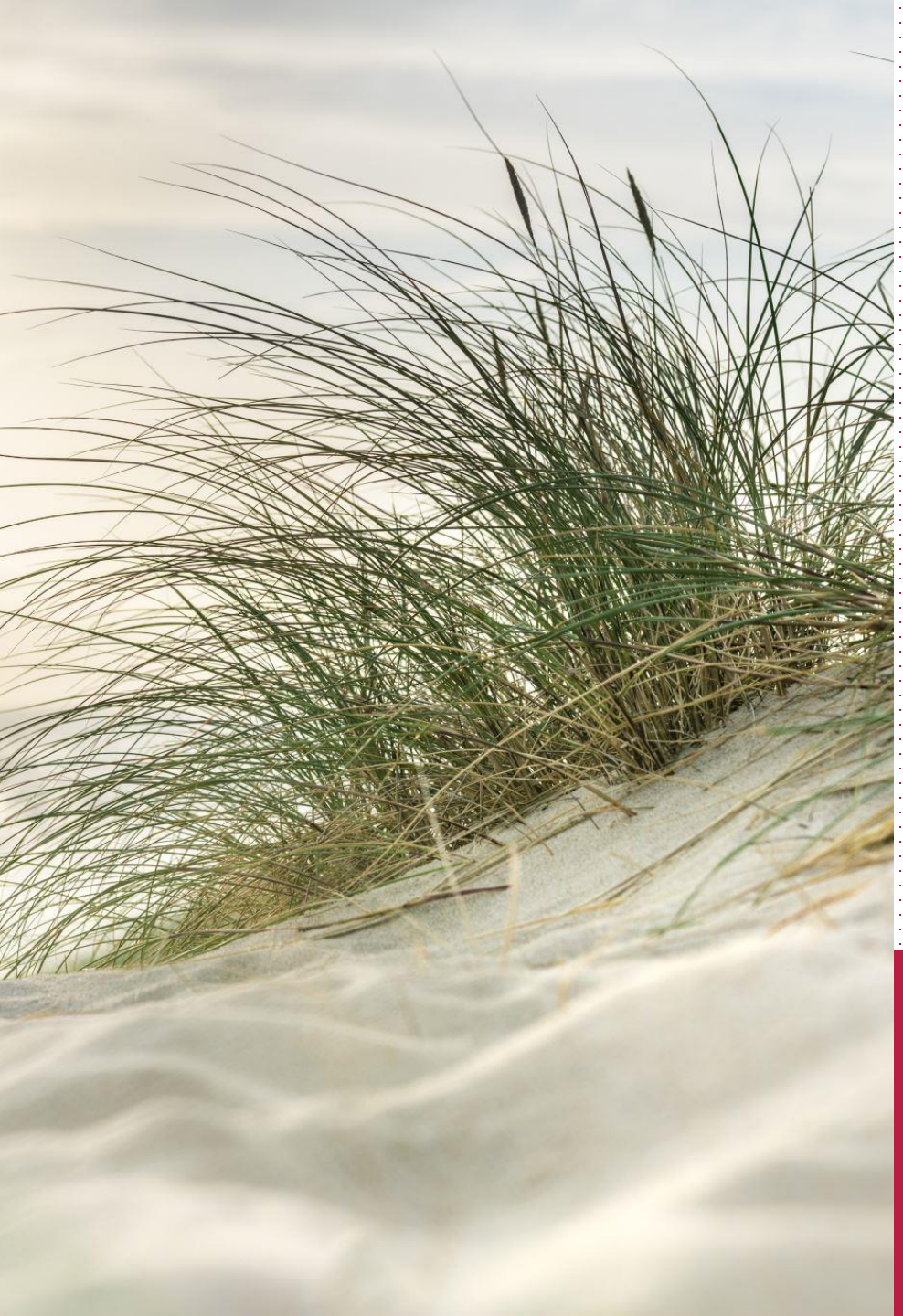

Effects of Vegetation and Wind on Assessing Coastal Dune Changes Using UAV and Total Station Surveys

Oreoluwa Adeniyi Osiberu[1,*], Jong-Won Choi[2], and Jianhong Jennifer Ren[1]
[1]Department of Environmental Engineering and [2]Department of Civil and Architectural Engineering, Texas A & M University- Kingsville, Kingsville, Texas
*Presenter

Overview

- Introduction
- Research Objectives
- Methodology
- Preliminary Results
- Preliminary Conclusions
- Selected References

Introduction

- Coastal areas are complex natural systems that are influenced by a variety of factors, such as water movement, sedimentation, morphology, biology, and human activity, at different spatial and temporal scales.
- According to recent United Nations reports, roughly 37% of the global population resides within a 100 km radius of the coast (Lapietra et al., 2022).
- Extreme environmental conditions including storm surges, high winds, and unusual tidal events exist in coastal regions.
- Coastal dune systems have been served as the first line of defense against the extreme weather conditions (Gonzalez, 2019).
- These coastal dunes are mounds of sand that are formed by aeolian processes, vegetation, and moisture (Abbate et al., 2019).

Introduction - Surveying of Coastal Dunes

- Surveying of coastal dunes - useful for monitoring impacts of sea-level rise, climate variations, and morphological changes, and for mapping, coastal research studies, and coastal management (Houser & Mathew, 2011).
- LiDAR dataset - for analysis of seasonal coastal erosion and accretion trend (Klemas, 2011; O'Dea et al., 2019).
- Total station surveys - for monitoring morphological changes in small area of a beach as recommended by Lee et al. (2013).
- Photogrammetric method - a reliable and affordable tool and used for assessing the evolution of embryo dunes (Taddia et al., 2019).

Objectives

- Quantify the temporal trends of survey-derived elevation models by applying and comparing three methods of data acquisition techniques i.e., LiDAR, Photogrammetry and Total Station.
- Examine the effects of wind and vegetation type on data acquisition using LiDAR, photogrammetry and total station.

Project Location

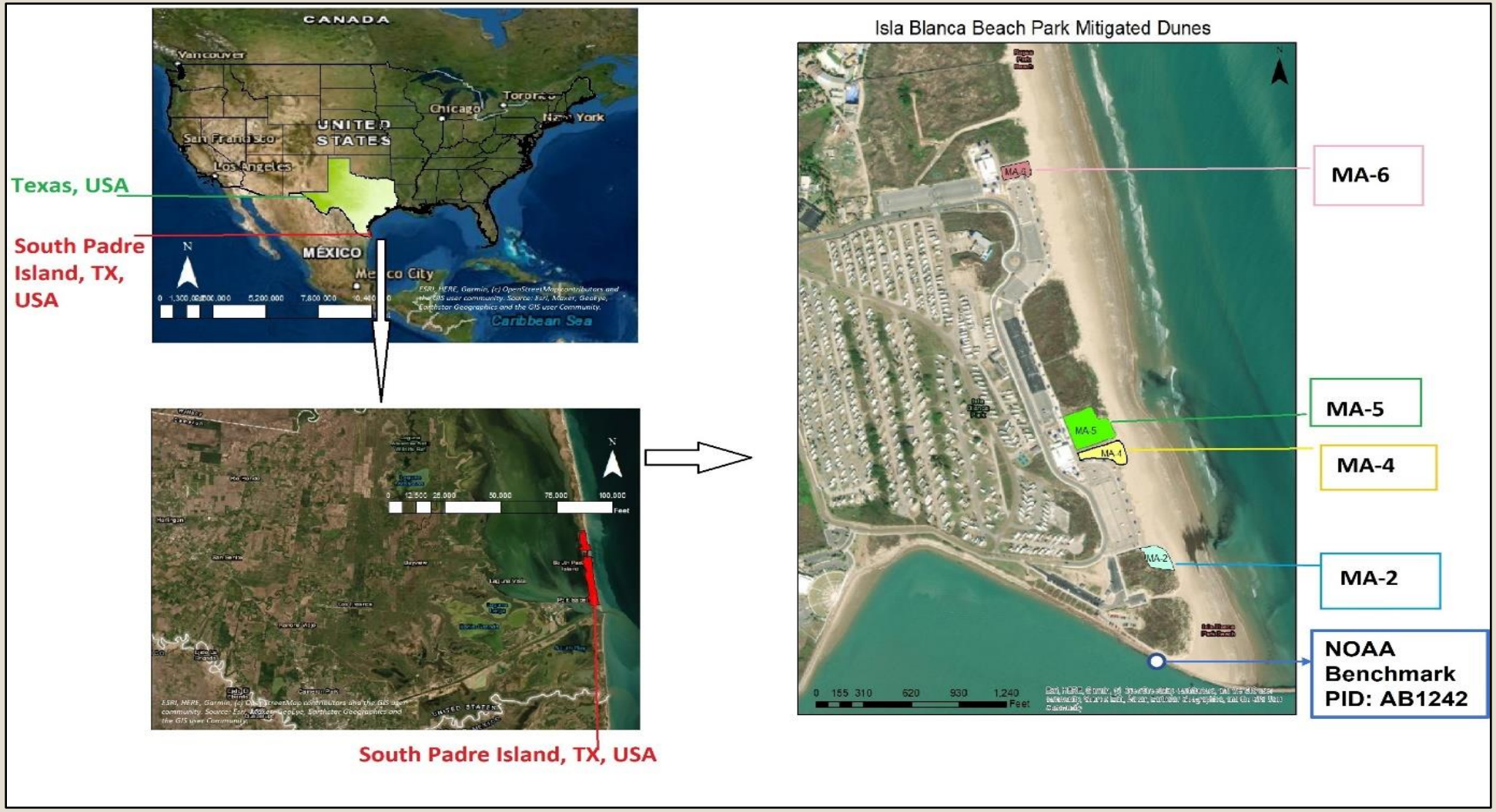

Figure 1: Project location, mitigation areas (MAs), and NOAA benchmark used for survey analysis at Isla Blanca Beach Park, South Padre Island, Texas, USA (Alayibo, 2022)

Materials and Methods - Total Station Surveys

- Topographic surveys - conducted using a Nikon NPL 322 model Total Station instrument
- NOAA benchmark station is located at an elevation of 1.427 m from the mean sea level with the coordinates of 26° 04' 05" N and 97° 09'20" W (NOAA, 2022)

Figure 2: Total Station set-up at Isla Blanca Beach Park, SPI, Texas, USA

Materials and Methods - Survey Details

- Data points was collected at every 1-meter horizontal interval on the toe of the dune and every 3-meter horizontal interval on top of the dune to better help understand the dynamics of the dune morphology

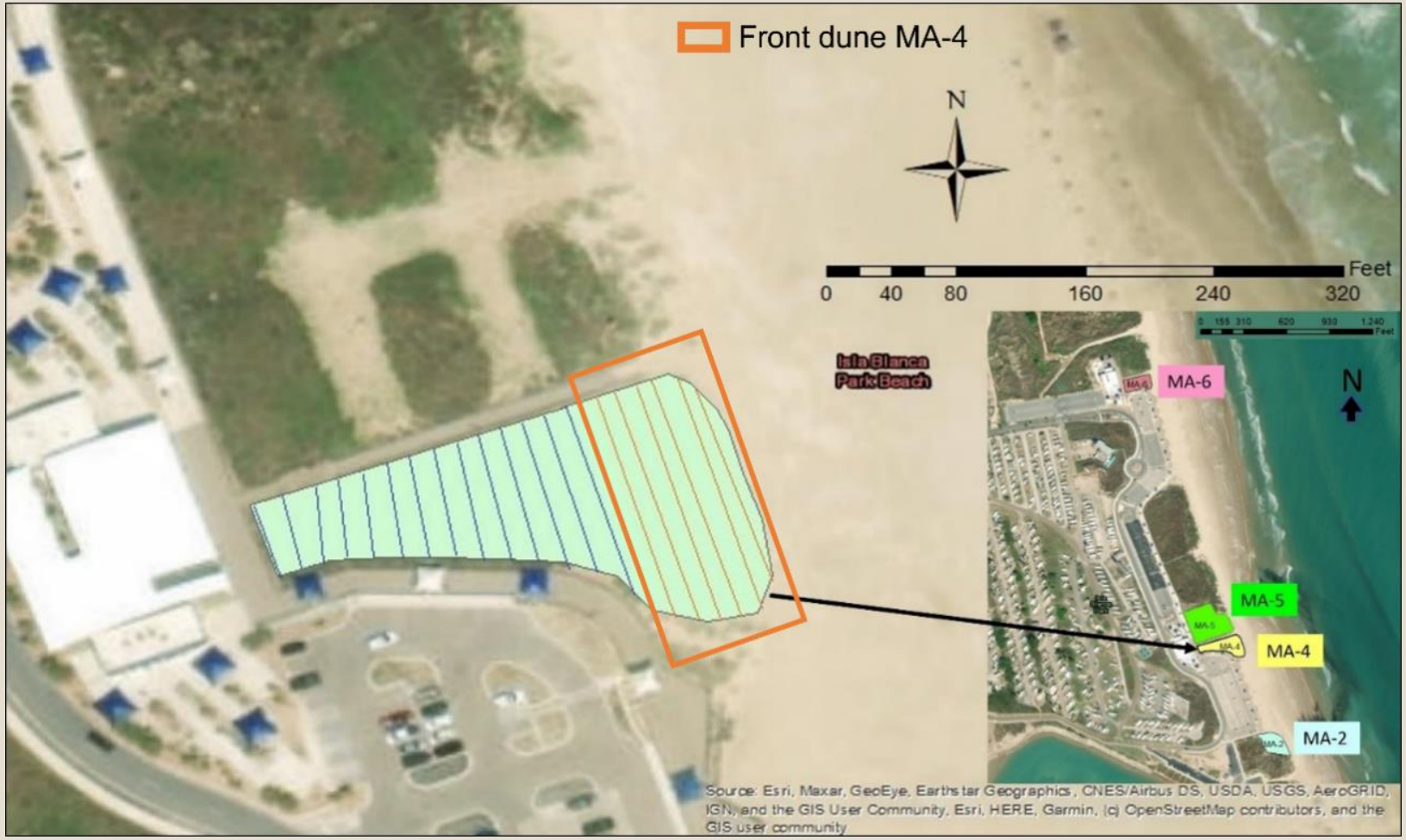

Figure 3: Survey profiles in MA-4 used in surveying dunes for volume estimations. Front dune section highlighted in orange box (Alayibo, 2022)

Materials and Methods – LiDAR Data

- LiDAR datasets - from Image Hunter LidarExplorer website (https://imagehunter.apollomapping.com) for the Fall of 2022 to the Spring of 2023.
- The availability of LiDAR data from this website offers a convenient and efficient means of accessing reliable geospatial information within the specified time frame.
- These datasets would be purchased at a cost.
- Only 2018 datasets are available on the National Map, which is the primary repository for USGS base geospatial data. We need concurrent datasets.

Materials and Methods – Data Comparison

- Root Mean Square Error (RMSE) (Equation 1) and Mean Absolute Difference (MAD) (Equation 2) - to quantify the differences of the derived datasets (Zimmerman et al., 2020)

$$\text{Root Mean Square Error (RMSE)} = \sqrt{\frac{\sum_{i=1}^{N}(Z_{i(UAS\ DEM)} - Z_{I(total\ station)})^2}{N}} \quad \textbf{(1)}$$

$$\text{Mean Absolute Difference (MAD)} = \sqrt{\frac{\sum_{i=1}^{N}|Z_{i(UAS\ DEM)} - Z_{I(total\ station)}|}{N}} \quad \textbf{(2)}$$

where:

- $Z_{UAS\ DEM}$ is the elevation coordinate measure by LiDAR
- $Z_{total\ station}$ is the elevation coordinate measure by total station
- n is the total number of check points used for the comparison

Materials and Methods – UAV Surveys

- A Preplanned flight plan is created in the Pix4D™ Capture App that encompass each survey area at a time.
- The flight altitude is set to 50 m above ground level, taking a picture every 2–4 s.
- The average spatial resolution of the images is set to 2.5 cm/pixel.

Figure 4: PARROT ANAFI used for image capturing

Materials and Method – UAV Data Processing

- A SfM algorithm is used to build a high-precision 3D terrain model from the UAV images collected.
- The workflow is divided into six steps (Bañón et al., 2019b):
    1) Add images
    2) Align photos
    3) Place markers
    4) Optimize camera alignment
    5) Build dense point cloud
    6) Generate DEM

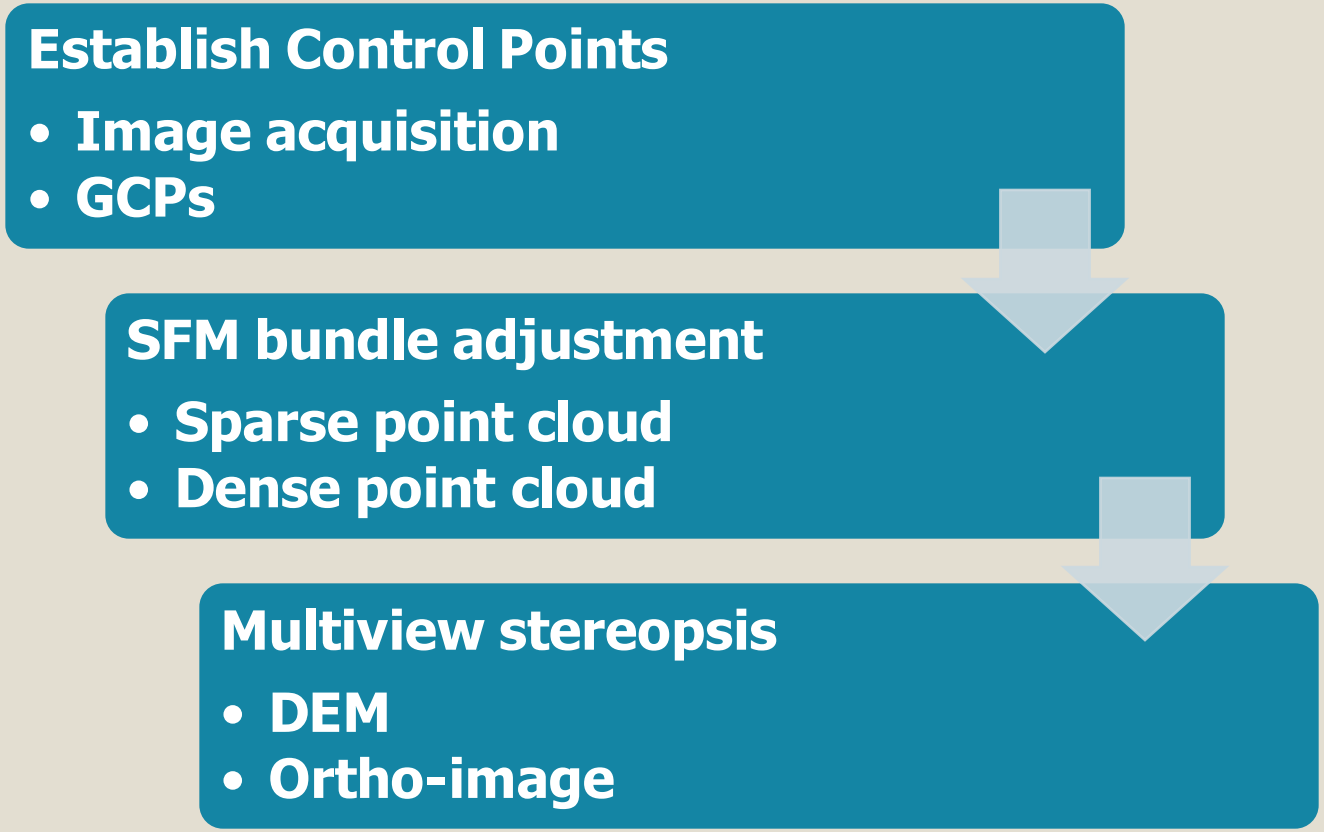

Figure 5: SfM workflow

Weather Station used for Wind Data Collection

- It provides reliable readings as weather conditions are continuously transmitted to cloud storage with the Ambient Weather Network.
- The in-situ wind data will be cross checked with prevailing wind conditions obtained from NOAA monitoring station (station 8779749) located close to the study area at Brazos Santiago Pass, SPI, Texas.

Figure 6: KestrelMet 6000 Weather station

Vegetation Assessment

- Carried out at all established UAV checkpoints .
- 1 m x 1 m quadrats sampling method.
- Native vegetation are counted by plant class (monocot and dicot) within quadrats.

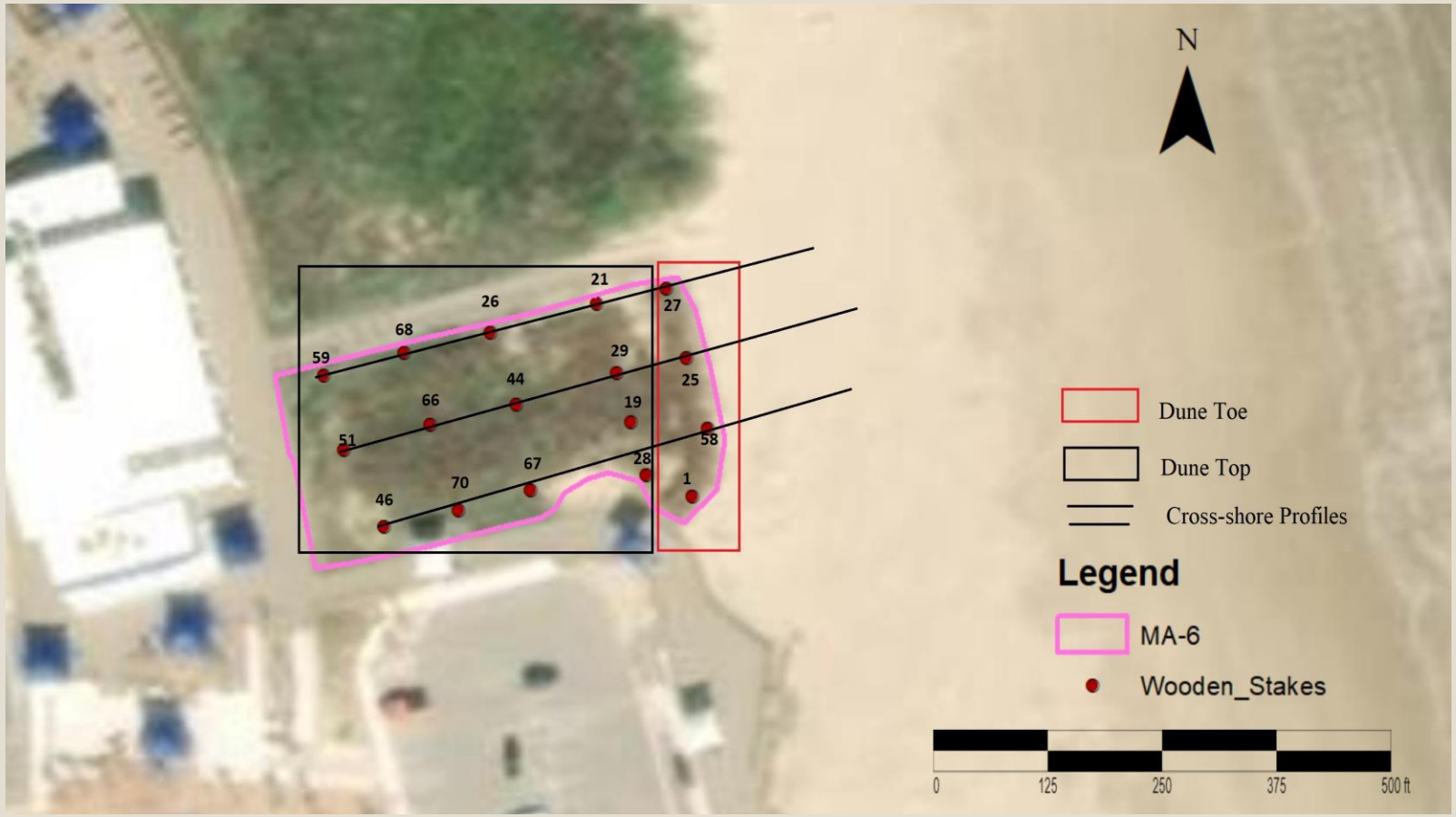

Figure 7: MA-6 Stakes location used for control points and vegetation assessment

Preliminary Results - 3D Models at MA-6

- The 3D models - generated using SURFER software from total station data collected from the field.
- A dataset comprising over 180 data points was gathered to construct these detailed models.
- A sequence of 3D surfaces - capture a key portion of foredune and landward transgressive dunes.

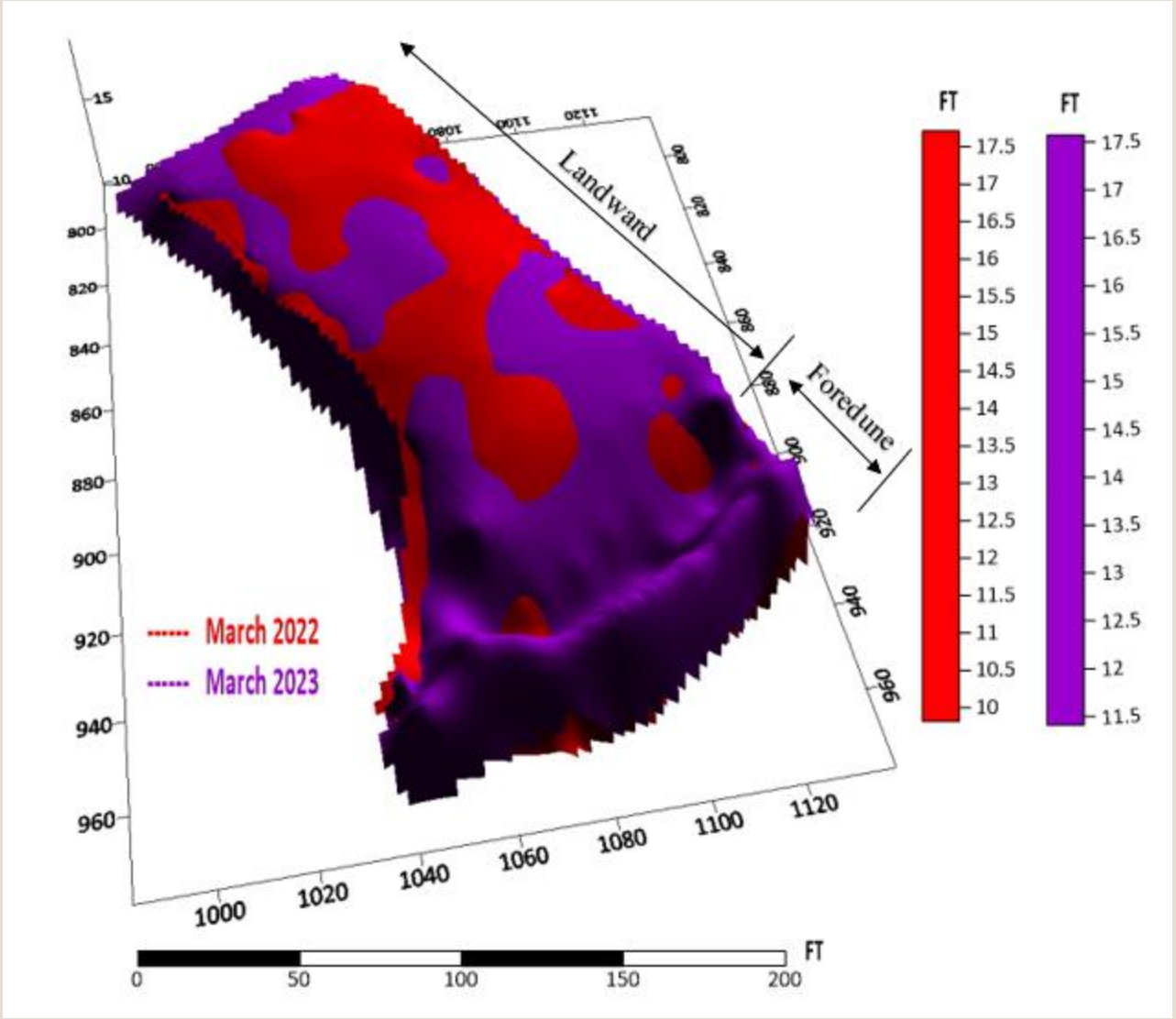

Figure 8: Overlayed MA-6 Digital elevation models

Preliminary Results - 3D Models at MA-4

- The data points were interpolated to create the surface representation using algorithms such as Kriging.

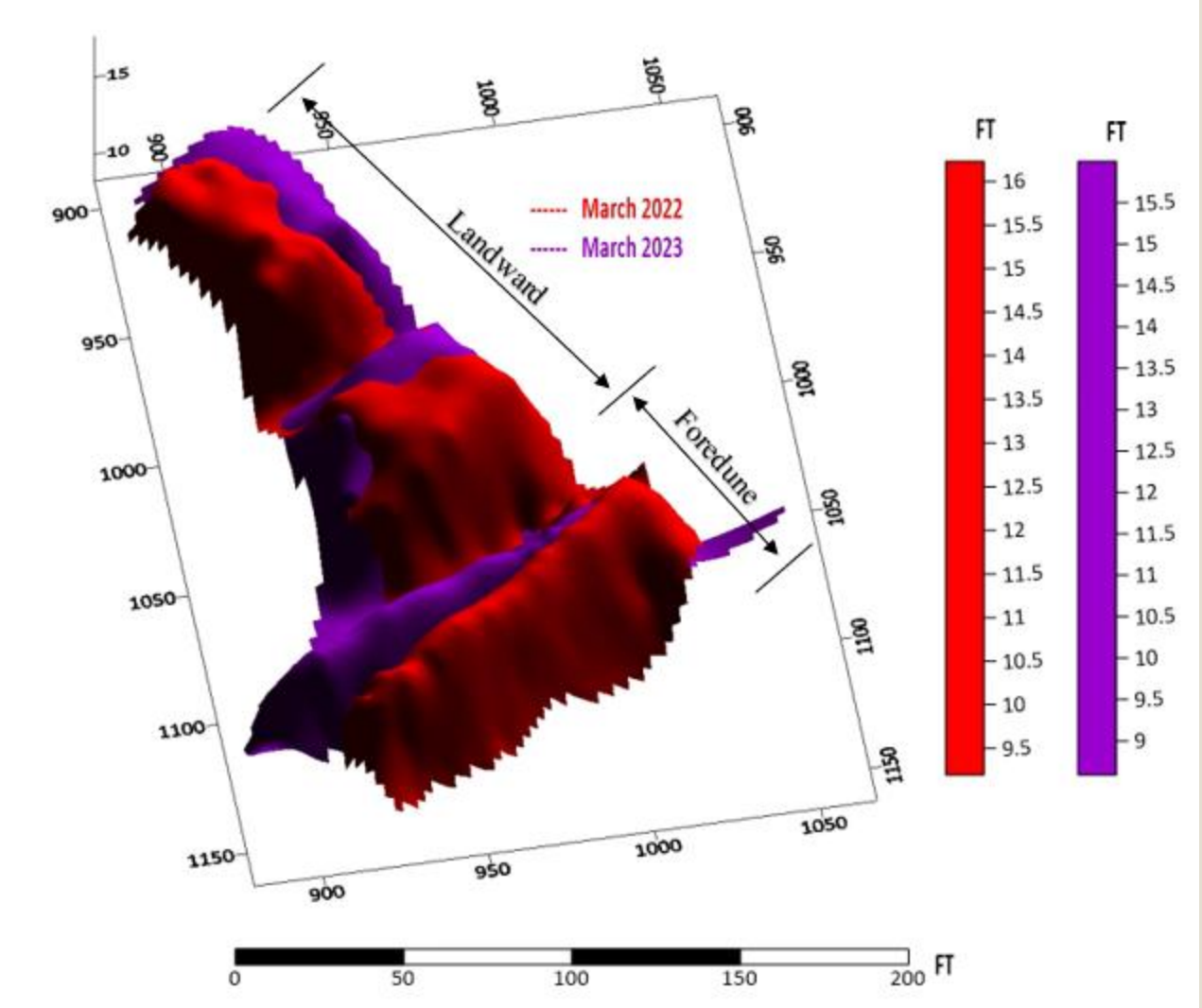

Figure 9: Overlayed MA-4 Digital elevation models

Cross-shore Profiles – MA-6

- The profiles were obtained using the SURFER software, by making a cross section of the elevation data in the middle of the dune.
- The profile demonstrates no change in foredune morphology but landward shows consistent lowering of parabolic dune deflation.

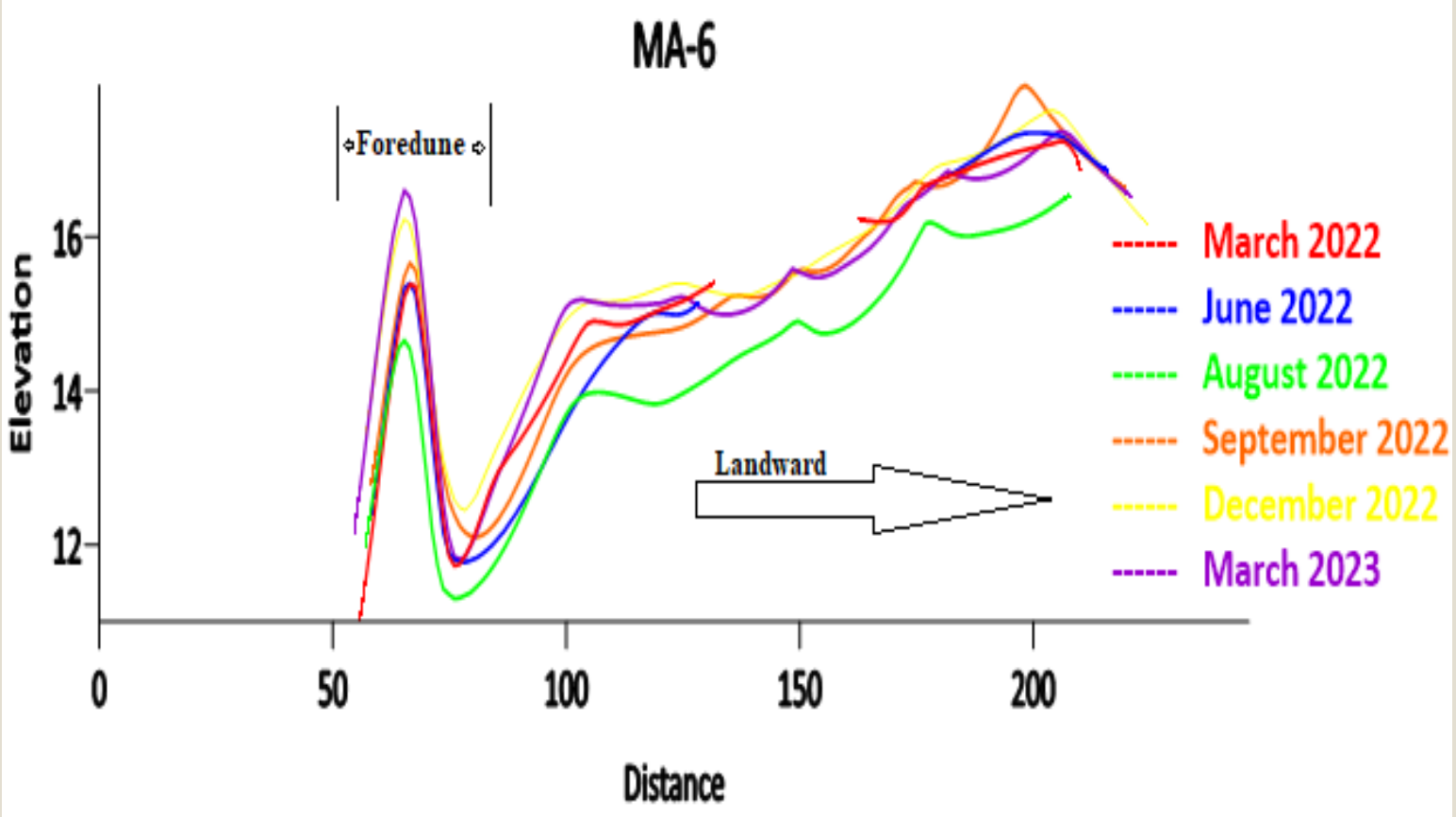

Figure 10: MA-6 2D Cross-shore profile generated with SURFER software using total station survey data

Cross-shore Profiles – MA-4

- The distance denoted in the x-axis represents the horizontal measurement along the perpendicular line of the cross-shore profile.
- Both distance and elevation are in feet.
- The profiles of the dune at MA-4 demonstrate an overall accumulation of sediment

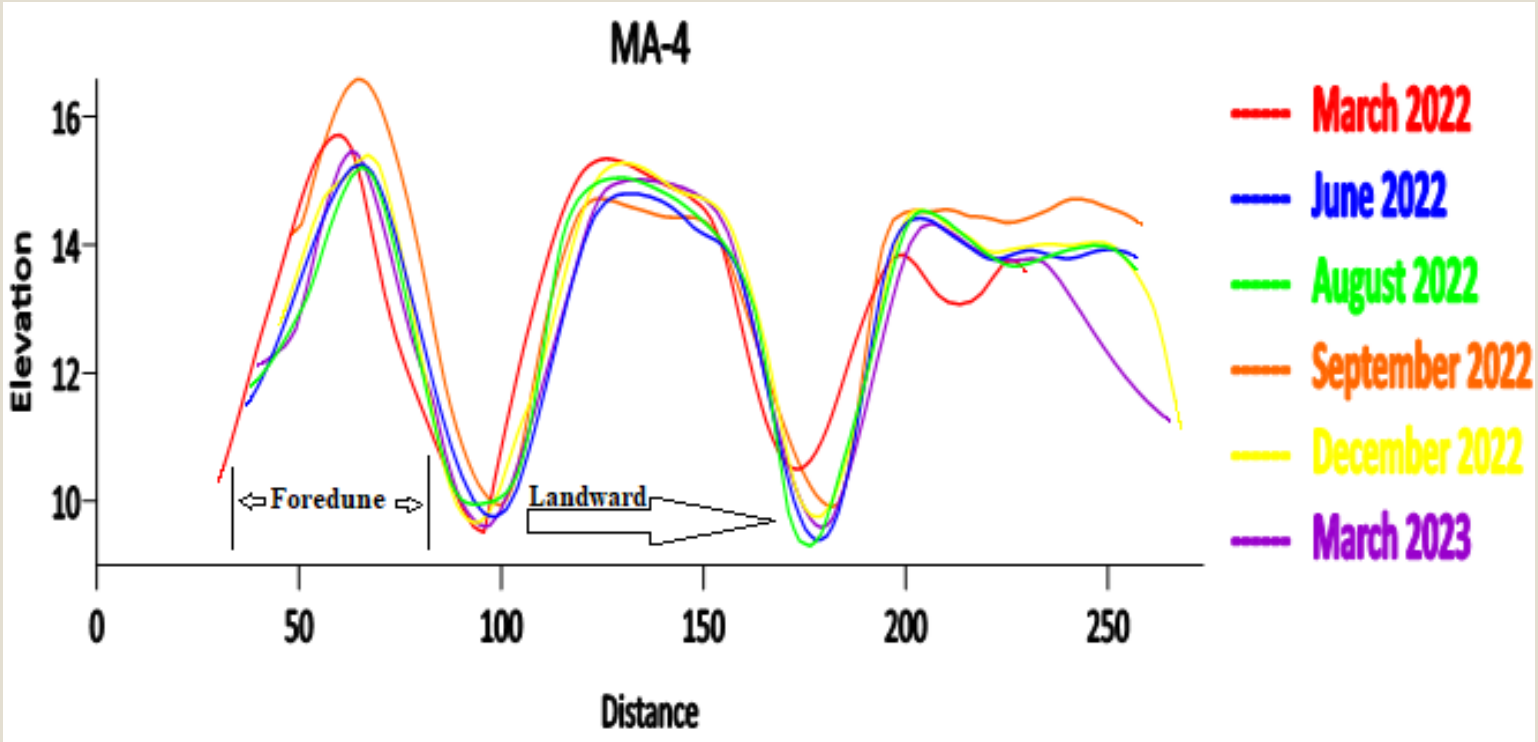

Figure 11: MA-4 2D Cross-shore profile generated with SURFER software using total station survey data

Orthomosaic Generated using Drone Data

- A total of 400 images were used to create the Digital Surface Model (DSM) and orthomosaic (Figure 12).
- The processing time, including computational tasks and adjustments, took about 24 hours.
- The resulting datasets had a consistent pixel resolution of 0.407 cm after accounting for the mosaicking and orthorectification.
- An assessment of the orthomosaic revealed a seamless integration of the images, resulting in accurate representation of the visual information in the orthomosaic.

Figure 12: MA-4 orthomosaic generated with PIX4DMAPPER software using drone data

Figure 13: MA-6 UAV survey error statistics generated with PIX4DMAPPER software using drone data

Ground Control Points

GCP Name	Accuracy XY/Z [US survey foot]	Error X [US survey foot]	Error Y [US survey foot]	Error Z [US survey foot]	Projection Error [pixel]	Verified/Marked
Q (BACK) (3D)	0.066/ 0.066	-0.004	0.006	-0.004	1.753	28 / 28
Q (MIDDLE) (3D)	0.066/ 0.066	0.013	-0.011	0.001	3.251	25 / 25
Q (FRONT) (3D)	0.066/ 0.066	-0.006	-0.001	0.012	3.930	23 / 23
Mean [US survey foot]		0.001283	-0.001831	0.002888		
Sigma [US survey foot]		0.008384	0.006915	0.006441		
RMS Error [US survey foot]		0.008482	0.007154	0.007059		

0 out of 14 check points have been labeled as inaccurate.

Check Point Name	Accuracy XY/Z [US survey foot]	Error X [US survey foot]	Error Y [US survey foot]	Error Z [US survey foot]	Projection Error [pixel]	Verified/Marked
stake 46		-0.0068	0.0237	0.0606	3.9025	24 / 24
Stake 70		-0.0374	0.0443	0.0920	3.1160	34 / 34
stake 67		-0.0086	0.0252	0.0256	3.3435	36 / 36
Stake 19		-0.0459	0.0465	0.1307	2.6533	31 / 31
Stake 51		0.0948	-0.0534	0.0294	2.0505	23 / 23
Stake 66		0.1368	-0.0833	-0.1006	2.2869	33 / 33
Stake 44		0.1724	-0.1028	0.2174	2.4257	34 / 34
Stake 29		0.0711	-0.0468	0.2093	2.9154	39 / 39
Stake 25		0.1538	-0.0875	0.3013	2.1736	22 / 23
Stake 59		0.0778	-0.0491	-0.0922	3.9975	11 / 11
Stake 68		0.1343	-0.0914	-0.1246	2.4675	23 / 23
Stake 21		0.1371	-0.0965	-0.1936	3.6623	26 / 26
Stake 27		0.1432	-0.1012	-0.0873	3.0240	17 / 17
Stake 26		0.1593	-0.1089	0.2964	3.4249	20 / 20
Mean [US survey foot]		0.084418	-0.048659	0.054582		
Sigma [US survey foot]		0.075010	0.056411	0.155380		
RMS Error [US survey foot]		0.112929	0.074497	0.164689		

Error Statistics Generated using GCPs

- The georeferencing had a total RMSE value of 0.007059 ft in elevation, relatively small, especially for a large number of images of different scales used to create the orthomosaic.
- The vertical accuracy of the DSM was more objectively assessed from check points independent of the dataset generation.

Ground Control Points

Figure 14: MA-4 UAV survey error statistics generated with PIX4DMAPPER software using drone data

GCP Name	Accuracy XY/Z [US survey foot]	Error X [US survey foot]	Error Y [US survey foot]	Error Z [US survey foot]	Projection Error [pixel]	Verified/Marked
Q1 (3D)	0.066/ 0.066	-0.034	0.176	0.215	2.419	27 / 27
Q2 (3D)	0.066/ 0.066	-0.093	0.085	0.046	2.004	45 / 45
Q3 (3D)	0.066/ 0.066	-0.036	-0.001	0.311	1.914	55 / 55
Q4 (3D)	0.066/ 0.066	0.111	-0.107	-0.214	2.285	39 / 39
Q5 (3D)	0.066/ 0.066	0.048	-0.151	-0.365	3.363	42 / 42
Mean [US survey foot]		-0.000798	0.000419	-0.001270		
Sigma [US survey foot]		0.071743	0.120104	0.254570		
RMS Error [US survey foot]		0.071747	0.120105	0.254574		

0 out of 20 check points have been labeled as inaccurate.

Check Point Name	Accuracy XY/Z [US survey foot]	Error X [US survey foot]	Error Y [US survey foot]	Error Z [US survey foot]	Projection Error [pixel]	Verified/Marked
Stake 3		0.0205	-0.2160	1.9264	0.9650	28 / 28
Stake 54		0.0238	-0.1673	1.1977	1.2751	34 / 34
stake 52		0.0214	-0.1085	0.8209	1.1004	36 / 36
Stake 39		0.0066	-0.0771	0.9146	0.8011	44 / 44
Stake 66		0.0051	-0.0524	0.1997	1.4360	47 / 47
Stake 1		0.0769	0.0055	0.0808	1.4609	26 / 26
stake 17		0.0177	-0.2688	-2.2811	0.8867	29 / 29
Stake 6		0.0442	-0.2212	-0.3881	0.9139	27 / 27
Stake 7		0.0102	-0.1837	1.6609	1.4102	38 / 38
Stake 8		0.0033	-0.1696	1.0947	2.0377	26 / 26
Stake 2		0.0580	-0.0864	-1.9273	1.3826	29 / 29
Stake 11		-0.0057	-0.0666	-3.5304	1.0307	40 / 40
Stake 35		-0.0553	-0.0624	-1.2063	1.6999	60 / 60
Stake 37		0.0389	0.0104	1.8495	1.5369	40 / 40
Stake 10		-0.0067	-0.2121	1.4822	2.3195	30 / 30
Stake 56		-0.0059	-0.1584	-0.6570	0.8677	15 / 15
Stake 38		-0.0178	-0.0908	1.2785	2.0678	32 / 32
Stake 22		-0.0005	-0.0414	0.6248	2.5364	25 / 25
Stake 55		-0.0108	-0.1355	1.3538	1.3739	15 / 15
Stake 42		-0.0514	-0.0396	0.2365	1.9719	38 / 38
Mean [US survey foot]		0.008626	-0.117093	0.236529		
Sigma [US survey foot]		0.031178	0.077611	1.457575		
RMS Error [US survey foot]		0.032349	0.140478	1.476642		

MA-4 UAV Survey Error Statistics

Positive values indicate that the elevations of points on the DSM surface are higher than the corresponding elevations of total station points, while negative values indicate the opposite, where the elevations of DSM points are lower than the corresponding total station points.

MA-6 DSM Generated using UAV Data

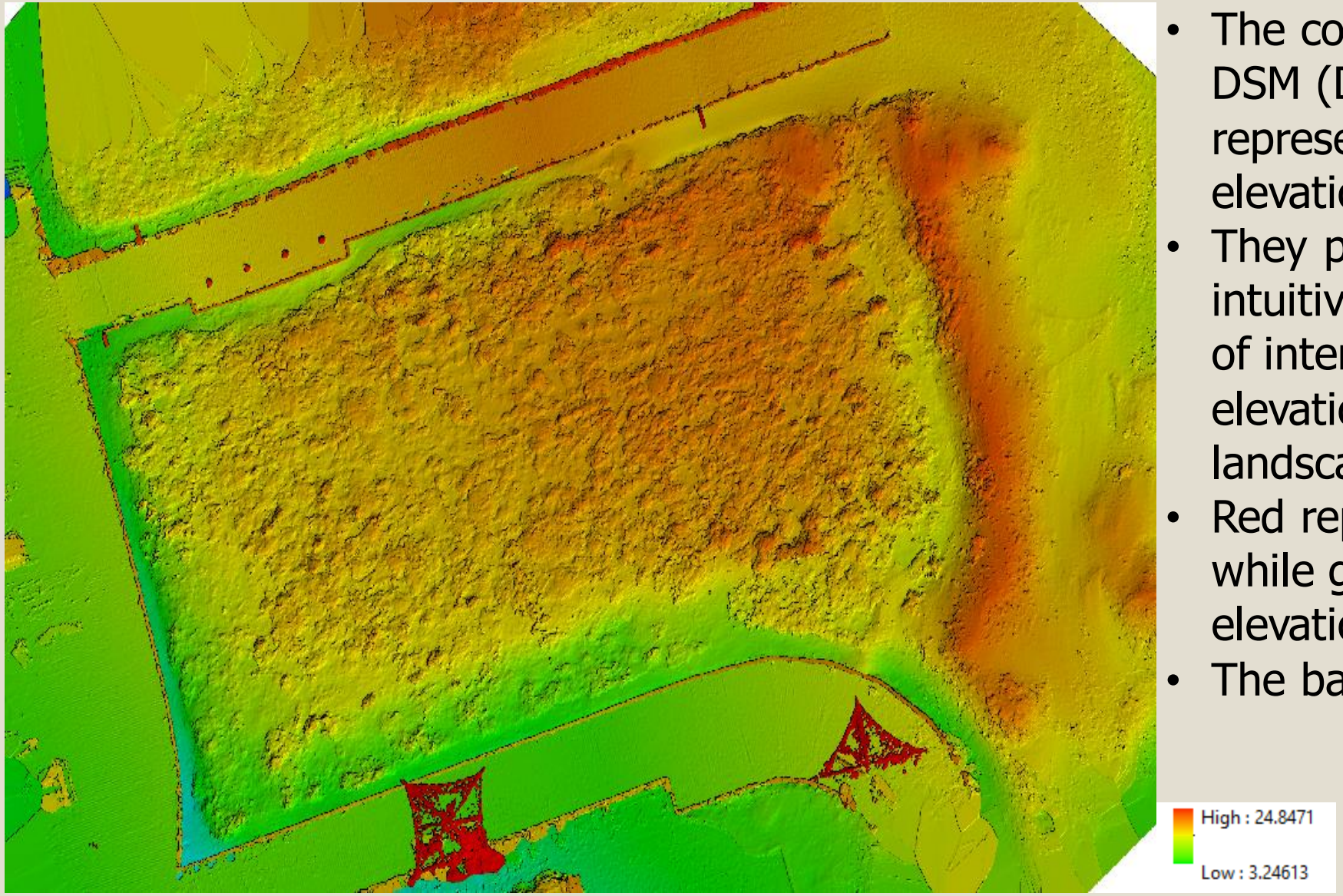

- The color differences in the DSM (Digital Surface Model) represent variations in elevation across the surface.
- They provide a quick and intuitive way to identify areas of interest and potential elevation variations in the landscape.
- Red represent higher elevation, while green depict lower elevation
- The band are represented in ft.

Figure 15: MA-6 DSM generated with PIX4DMAPPER software using drone data

Preliminary Conclusions

- The survey data collected here will capture broader landscape dynamics of an active dune characterized by foredune.
- A more dynamic and resilient biogeomorphic system can be achieved through coastal dune restoration projects.
- Preliminary findings suggest that the use of UAVs, LiDAR, and total station surveys offer distinct advantages in monitoring coastal restoration.
- UAV surveys prove effective in capturing high-resolution imagery, while total station surveys provide precise elevation measurements, especially in areas with dense vegetation.

Acknowledgements

- Project funding is provided by Texas General Land Office, Coastal Management Program, Contract: 22-045-008-D105; and Cameron County, Texas.
- Teammates- Alayibo Semenitari, Juan Rodriguez, and Anthony Ramon

Selected References

- Abbate, A., Campbell, J. W., Kimmel, C. B., & Kern, W. H. (2019). Urban development decreases bee abundance and diversity within coastal dune systems. Global Ecology and Conservation, 20, e00711. https://doi.org/10.1016/j.gecco.2019.e00711
- Bemis, S. P., Micklethwaite, S., Turner, D., James, M. R., Akciz, S., Thiele, S. T., & Bangash, H. A. (2014). Ground-based and UAV-Based photogrammetry: A multi-scale, high-resolution mapping tool for structural geology and paleoseismology. Journal of Structural Geology, 69, 163–178. https://doi.org/10.1016/j.jsg.2014.10.007
- Houser, C., & Mathew, S. (2011). Alongshore variation in foredune height in response to transport potential and sediment supply: South Padre Island, Texas. Geomorphology, 125(1), 62–72. https://doi.org/10.1016/j.geomorph.2010.07.028
- Klemas, V. (2011). Beach Profiling and LIDAR Bathymetry: An Overview with Case Studies. Journal of Coastal Research, 277, 1019–1028. https://doi.org/10.2112/JCOASTRES-D-11-00017.1
- Lapietra, I., Lisco, S., Capozzoli, L., De Giosa, F., Mastronuzzi, G., Mele, D., Milli, S., Romano, G., Sabatier, F., Scardino, G., & Moretti, M. (2022). A Potential Beach Monitoring Based on Integrated Methods. Journal of Marine Science and Engineering, 10(12), 1949. https://doi.org/10.3390/jmse10121949
- Lee, J.-M., Park, J.-Y., & Choi, J.-Y. (2013). Evaluation of Sub-aerial Topographic Surveying Techniques Using Total Station and RTK-GPS for Applications in Macrotidal Sand Beach Environment. Journal of Coastal Research, 65, 535–540. https://doi.org/10.2112/SI65-091.1
- Taddia, Y., Corbau, C., Zambello, E., & Pellegrinelli, A. (2019). UAVs for StructureFrom-Motion Coastal Monitoring: A Case Study to Assess the Evolution of Embryo Dunes over a Two-Year Time Frame in the Po River Delta, Italy. Sensors, 19(7), 1717. https://doi.org/10.3390/s19071717